Int. J. Heat Mass Transfer. Vol. 35, No. 1, pp. 155–164, 1992
Printed in Great Britain

0017–9310/92 $5.00 + 0.00
© 1991 Pergamon Press plc

Natural convection in honeycomb wall spaces

G. S. H. LOCK and LITONG ZHAO
Department of Mechanical Engineering, University of Alberta, Edmonton, Alberta, Canada T6G 2G8

(*Received* 19 *April* 1990 *and in final form* 3 *January* 1991)

Abstract—The results of a numerical study of laminar, natural convection in a honeycomb wall filled with air spaces are presented. The study attempts to compare the honeycomb wall with the conventional wall cavity filled with common porous materials. Using discretized forms of the governing differential equations, heat transfer data are obtained for two different cavities: square and triangular cross sections, both having an aspect ratio of 5 : 1. The data are plotted in the form of Nusselt number vs Rayleigh number. Three flow regimes are evident. The effect of rotation of the cavity about its longitudinal axis is examined along with the effect of tilting the longitudinal axis above and below the horizontal. The triangular cavity tilted with the higher temperature at the upper end is found to have insulation properties comparable with conventional wall fillings.

INTRODUCTION

INTERNAL temperature control and energy conservation are both important aspects of building design, and both are dependent on the heat transfer processes which are operative in and on the building envelope. In turn, heat transfer rates across the envelope are determined by the conductive, convective and radiative characteristics of the envelope space, as defined by its thickness and the arrangements of the structural and non-structural elements it contains.

Heat transfer across wall spaces, floor spaces and roof spaces is often the combined result of conduction and convection in the cavities and pores of air formed by the chosen design; the space between the inner and outer (planar) shells may or may not be subdivided by studs or cross pieces; and it may or may not be filled with foamed or granular insulation. Typically, the contribution of radiation is small in these spaces but the same would not generally be true for fittings such as double-glazed windows and skylights; nor would it be true for solar collectors.

Among various strategies to improve the insulating properties of envelope cavities is the use of honeycombing. This approach has been the subject of much attention in the last two decades. Catton [1] summarized a number of studies dealing with circular, hexagonal, square and rectangular honeycombs. Of particular importance is the experimental work of Cane *et al.* [2] on square sections, and the related study of Arnold *et al.* [3] on rectangular sections. Trefethen and Chung [4] described experiments with a venetian blind geometry and later complemented their work with a two-dimensional analysis [5]. At about the same time, Eftekhar *et al.* [6] suggested a simplified analytical model for quasi-one-dimensional heat conduction through a wall built from square honeycomb cavities.

Very recent work at the University of Alberta has also been directed towards the behaviour of honeycomb wall spaces. The results of a numerical study of the square honeycomb cavity with its longitudinal axis horizontal are presented in ref. [7], while the effect of inclining the cavity above and below the horizontal is described in ref. [8].

The present work is a comparative numerical study of two honeycomb cross sections: a square and a triangle formed by halving the square through the diagonal. Previous work on triangular-section cavities appears to have been limited to two dimensions [9–11]. Here, the analysis is extended to three-dimensional heat transfer in a cavity with an aspect ratio of 5 : 1. The study will be limited to steady, laminar conditions in air, and neglects radiation. In addition to examining the effect of section geometry, it will give consideration to the effects of inclination, both in respect to rotation of the cavity about its longitudinal axis (here described as roll) and in respect to inclination of the long axis relative to the horizontal (here described as tilt). Comparisons will be made with cavities filled with conventional insulating materials.

FORMULATION

A rectangular coordinate system was chosen and is defined in Fig. 1. For either the square or triangular section; the longitudinal (X) axis is the axis about which roll displacements take place. In the configuration shown, the Y-axis is parallel to the gravitational acceleration vector and the Z-axis is then the tilt axis. In general, the tilt axis is always normal to the roll axis but the plane containing them both will not always be horizontal. For ease of reference, the tilt and roll angles were measured as follows. Tilt (α) was taken with respect to a horizontal roll axis, positive angles indicating that the hotter end of the cavity ($X = 0$) is the lower end. Roll (γ) was taken with respect to a horizontal diagonal, with the vertex being

NOMENCLATURE

A	end area [m^2]
D	cavity width [m]
g	gravitational acceleration [$m\ s^{-2}$]
k	thermal conductivity [$W\ m^{-1}\ K^{-1}$]
L	cavity length [m]
Nu	Nusselt number
P	absolute pressure [Pa]
Q	heat flux [W]
Ra	Rayleigh number
T	absolute temperature [K]
U, V, W	velocities in the X-, Y-, Z-direction, respectively
X, Y, Z	rectangular coordinates.

Greek symbols

α	tilt angle
β	thermal expansion coefficient [K^{-1}]
γ	roll angle
κ	thermal diffusivity [$m^2\ s^{-1}$]
ν	momentum diffusivity [$m^2\ s^{-1}$]
ρ	density [$kg\ m^{-3}$]
ϕ	normalized temperature.

Subscripts

eff	effective
H, C, m	hot, cold and central planes, respectively
x, y, z	differentiation with respect to x, y, z, respectively.

above for a triangular section; symmetry then dictates that equal positive and negative roll angles produce the same effect.

As indicated in Fig. 1, the aspect ratio of the cavity is L/D which was fixed at 5 : 1 for all the results presented. The triangular section is seen to be right-angled with the short sides being equal to each other and to the square side. These geometrical characteristics were believed to be suitable for the main purpose of the study and provided useful comparisons with other work.

Buoyant flow within the cavity is governed by the differential equations of motion, continuity and energy. These may be written in their primitive form using the Cartesian coordinate system. Following the introduction of non-dimensional variables they become

$$\left.\begin{aligned}
&u_x+v_y+w_z=0\\
&uu_x+vu_y+wu_z=-\left(\frac{D}{L}\right)^2p_x+\left(\frac{D}{L}\right)\phi\sin\alpha\\
&\qquad+\left(\frac{2Pr}{Ra}\right)^{1/2}\left[\left(\frac{D}{L}\right)^2u_{xx}+u_{yy}+u_{zz}\right]\\
&uv_x+vv_y+wv_z=-p_y+\phi\cos(\gamma-3\pi/4)\cos\alpha\\
&\qquad+\left(\frac{2Pr}{Ra}\right)^{1/2}\left[\left(\frac{D}{L}\right)^2v_{xx}+v_{yy}+v_{zz}\right]\\
&uw_x+vw_y+ww_z=-p_z+\phi\sin(\gamma-3\pi/4)\cos\alpha\\
&\qquad+\left(\frac{2Pr}{Ra}\right)^{1/2}\left[\left(\frac{D}{L}\right)^2w_{xx}+w_{yy}+w_{zz}\right]
\end{aligned}\right\}\quad(1)$$

and

$$u\phi_x+v\phi_y+w\phi_z=\left(\frac{2}{Ra\,Pr}\right)^{1/2}\times\left[\left(\frac{D}{L}\right)^2\phi_{xx}+\phi_{yy}+\phi_{zz}\right]$$

in which

$$x=X/L,\quad y=Y/D,\quad z=Z/D$$

$$u=DU/L\sqrt{F},\quad v=V/\sqrt{F},\quad w=W/\sqrt{F}$$

where $F=\beta g(T_H-T_m)D$, β is the coefficient of expansion for air, g the gravitational acceleration, T_H the temperature of the hotter end wall and T_m the wall temperature in the central plane $X=L/2$. The pressure and temperature are rendered non-dimensional by

$$p=P/\rho F\quad\text{and}\quad\phi=\frac{T-T_m}{T_H-T_m}.$$

The Prandtl number, $Pr=\nu/\kappa$, is here fixed at $Pr=0.71$. The walls of the cavity were taken to be rigid and impermeable. Hence the hydrodynamic

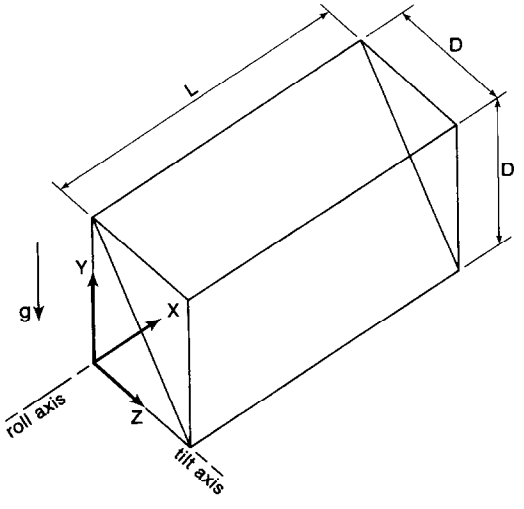

FIG. 1. Coordinate system.

boundary conditions on equations (1) are $u = v = w = 0$ on all bounding surfaces. The end walls were taken as isothermal; that is

$$\phi(0, y, z) = 1$$

$$\phi(1, y, z) = -1.$$

For the long walls, two separate thermal conditions seem appropriate to a honeycomb cavity: a linear temperature distribution $\phi = 1 - 2x$ simulating a perfectly conducting wall; and an adiabatic condition simulating a non-conducting wall. In practice, the role of conduction in the wall would depend principally on the ratio (r_k) of the wall conductivity and the fluid (air) conductivity. As $r_k \to \infty$, the linear wall temperature condition is approached, while as $r_k \to 0$, the adiabatic condition prevails. Most of the results presented here have been obtained with a linear wall temperature distribution.

The equations were discretized and solved using the finite difference algorithm of Patankar [12] in the SIMPLE-C version suggested by Van Doormaal and Raithby [13]. Iteration was continued until a convergence criterion had been satisfied. This consisted of the requirement that successive averaged values of the dependent variables agree to within 1%; agreement was frequently better than this.

Typically, a run would require no more than 100 iterations using a $51 \times 13 \times 13$ mesh. The initial fields were taken as zero, nominally, although a few runs were repeated with other initial conditions to confirm that the solution was unique.

As a matter of convenience, the nodal networks used for the square and triangular sections were identical. This choice followed a variety of numerical experiments including alignment of the coordinate system with the diagonal. Although the sawtooth boundary representing the diagonal introduces some error, its effect on the diagonal heat flux distribution was found to be minor. The triangular section results were thus obtained by suppressing all velocity and temperature variations on one side of the diagonal. This was done using a large source in each of the nodal equations to be eliminated.

Before the data proper were generated the programme was validated and the accuracy estimated. Validation was undertaken both qualitatively and quantitatively, the former consisting of replication of established two-dimensional secondary and tertiary behaviour [14, 15]. Quantitative comparisons were also made with the Nusselt numbers generated in the related three-dimensional study of Mallinson and de Vahl Davis [16]. Based upon these validation studies, and a comparison of additional current data obtained with $51 \times 11 \times 11$, $61 \times 13 \times 13$ and $71 \times 15 \times 15$ networks, it is estimated that the Nusselt numbers presented have an accuracy of about 5%.

RESULTS AND DISCUSSION

Recent work [7, 17] has revealed the basic flow pattern in a slender horizontal cavity exposed to different end temperatures. This consists of a simple primary loop upon which is superimposed a secondary circulation induced by lateral temperature gradients. It is to be expected that the precise details of the flow would depend upon the temperature distribution over the long surfaces and, for a non-circular cross section, upon the geometry and roll angle of the cavity.

Figure 2 shows the two-filament primary flow in the horizontal square-section cavity when $\gamma = \pi/4$, $Ra = 10^5$, and the wall temperature varies linearly. This longitudinal velocity profile is seen to take its familiar S-shape which is only slightly modified by the side walls. The form is preserved in tilted cavities provided they are not too close to the vertical [8, 18]. The corresponding secondary flow is revealed through the transverse velocity field on selected planes in Fig. 3. The bar on the left-hand side indicates the non-dimensional velocity scale. In the central plane ($x = 0.5$), the anticipated two-fold symmetry is evident in a pair of vortex pairs. The symmetry about the vertical mid-plane is retained as the cavity end is approached but the vortex pairs become increasingly unequal until they are replaced by the refluent end flow. At this Rayleigh number, the end flow is restricted to a region extending about half the cavity width from the end.

The effect of rolling the cavity about its longitudinal axis is indicated in Fig. 4 which, together with the bottom right-hand diagram of Fig. 3, shows the transverse velocity field in the central plane. As expected, the flow pattern exhibits a two-fold symmetry for the limiting roll angles of $\gamma = 0$ and $\pi/4$. Between these limits the four vortices must somehow find accommodation with the 'unsymmetric' section geometry. The intermediate roll angles chosen here provide a representative illustration of the flow adjustment.

A similar study was undertaken for the triangular cross section with the longitudinal axis again being horizontal and the Rayleigh number remaining at 10^5. Figure 5 illustrates the primary flow when the diagonal is horizontal. As indicated, the opposed filaments adjust their cross-sectional area to fit the triangular geometry and reach very close to the end before the turn begins. The accompanying secondary flow is shown in Fig. 6 which reveals how the two vortex pairs adjust to the non-rectangular geometry and vanish in the end region. Again the bar on the left-hand side indicates the non-dimensional velocity scale. Under these conditions, the basic elements of the flow pattern previously observed are preserved; only the details are altered to fit the section geometry.

Rolling the triangular section about the longitudinal (horizontal) axis produced the mid-plane results shown in Figs. 6(d), 7(a) and (b) for $Ra = 10^5$. As expected, the transverse field exhibits symmetry about the mid-plane passing through the vertex when $\gamma = 0$ or $\pi/2$. However, the flow patterns at these limiting roll angles are substantially different. It is clear that the diagonal, as the longest side, plays a sig-

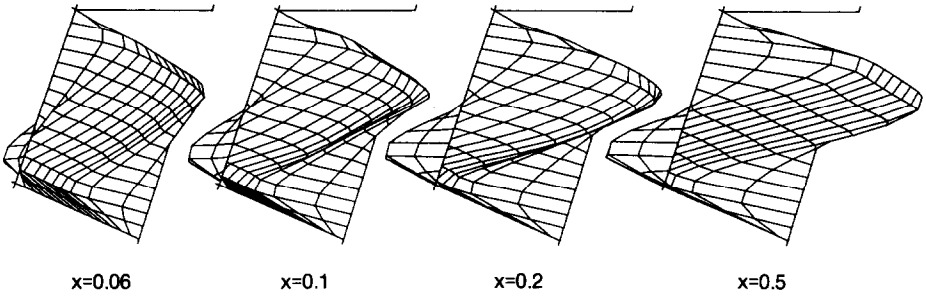

FIG. 2. Primary flow in a horizontal square section cavity viewed from below: $Ra = 10^5$.

nificant part. When the diagonal is horizontal, the flow adjacent to it is very weak and the effect of vortical motion is felt mainly along the shorter sides. A vertical diagonal evidently creates a very different situation in which a stronger vortical motion fills the entire cross section.

The intermediate roll angle $\gamma = \pi/4$ creates a particularly interesting result which is also shown in Fig. 7. For the higher Rayleigh number of 10^6, four unequal vortices are evident, each adjusting to the shape of its neighbours and the local wall geometry; this is shown in Fig. 7(d). However, for $Ra = 10^4$ the interplay of internal boundaries produces an alteration in the flow pattern, as indicated in Fig. 7(c). In the region originally common to the top vortices and the lower right vortex, the velocity vectors have become mutually reinforcing and have generated a strong field moving up left. On the other hand, the region common to the bottom vortices and the upper left vortex has been occupied by a strong field moving down right. That is, the vortices originally positioned top left and bottom right in Fig. 7(d) have almost merged into a single counterclockwise vortex separating unequal, and weaker, clockwise vortices positioned up right and down left. This behaviour suggests that other cavity geometries may, by virtue

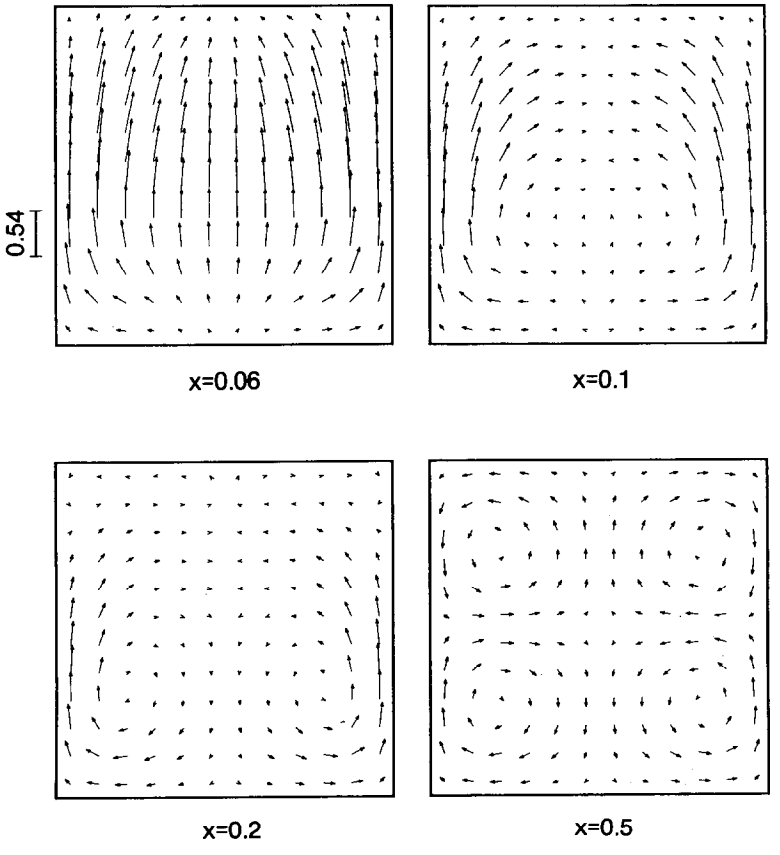

FIG. 3. Secondary flow in a horizontal square section cavity: $Ra = 10^5$.

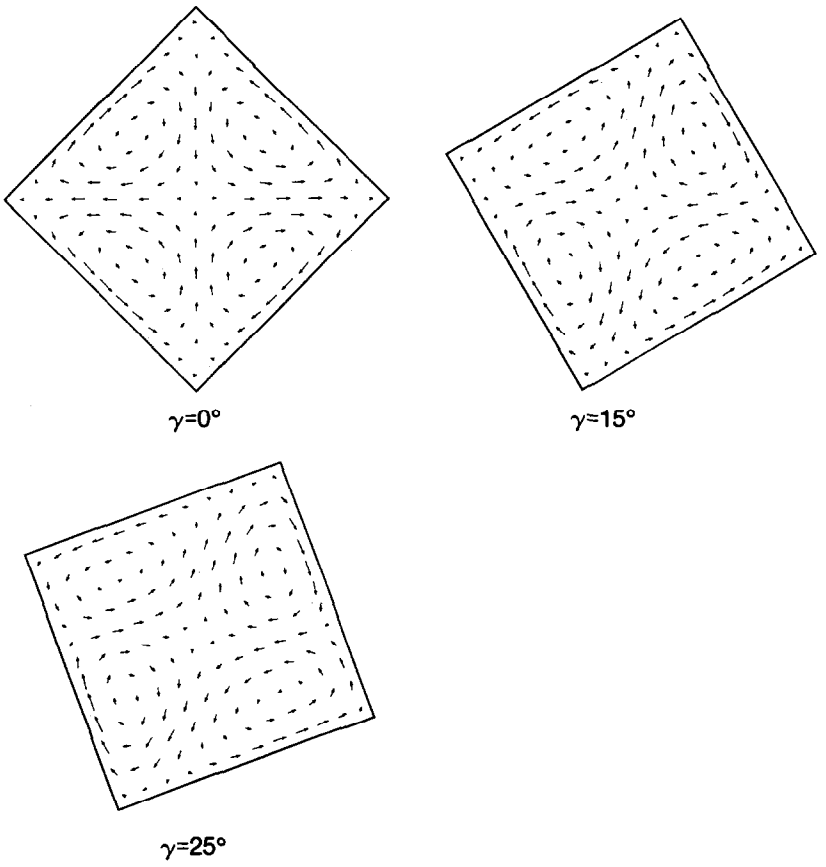

FIG. 4. Effect of roll on secondary flow in the central plane of a horizontal, square section cavity: $Ra = 10^5$.

of their shape and orientation, produce departures from the basic four vortex flow pattern, depending upon the Rayleigh number.

Heat transfer characteristics

The rate of heat transfer through a cavity may be defined in several ways the most appropriate of which, for present purposes, is to base it on the end walls. Accordingly, the Nusselt number of the cavity has been defined by

$$Nu = \frac{QL}{A(T_H - T_C)k}$$

in which Q is the heat flux over the end wall, k the thermal conductivity of air and A the area of the end wall (D^2 and $D^2/2$ for the square and triangular sections, respectively). In general, Nu will be a function of the cavity geometry and orientation. It will also depend upon the Rayleigh number, defined by

$$Ra = \frac{\beta g(T_H - T_C)D^3}{\nu\kappa}$$

where ν and κ are the momentum diffusivity and thermal diffusivity, respectively. A representative indication of this dependency is shown by the open symbols in Fig. 8 for square and triangular cavities lying horizontally. It is evident that when $Ra \lesssim 10^4$ the systems behave essentially as pure air conductors, in

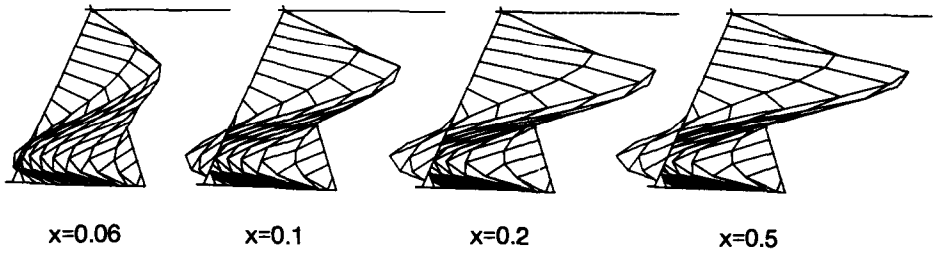

FIG. 5. Primary flow in a horizontal, triangular section cavity viewed from below: $Ra = 10^5$.

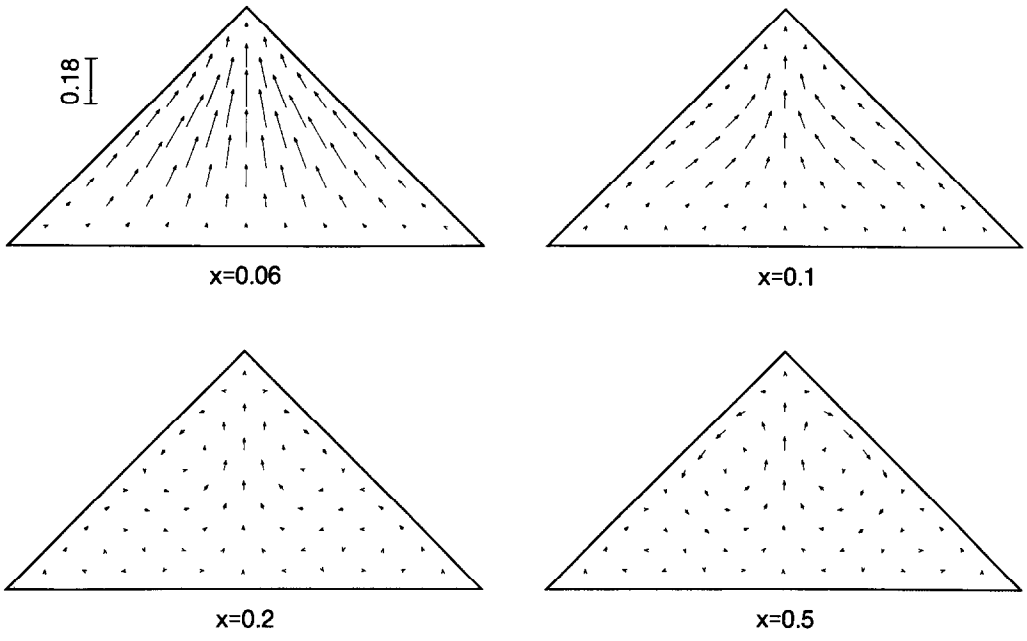

FIG. 6. Secondary flow in a horizontal, triangular section cavity: $Ra = 10^5$.

which condition they would be effective insulators. It is also clear that as Ra increases beyond 10^4 the growth of convection increases the heat transfer rate, first steeply and subsequently with less effect. For Rayleigh numbers in excess of 10^6, it appears that a boundary layer type of flow may exist around the walls of the cavity with velocity and temperature gradients in the central core region being relatively small. As Ra falls below 10^6, the boundary layers evidently grow to fill the cavity thus leading to an 'impeded' regime in which interference between the outer and inner flows creates comparable lateral gradients in both. The corresponding reduction in heat transfer rate eventually leads to the conduction regime in which, although convection does not cease entirely, the temperature field does cease to be dependent on it. From the point of view of thermal insulation, this is the preferred regime. Its upper limit is a function of system parameters and is discussed at length below.

Heat transfer data for the square cavity with a linearly varying wall temperature are displayed in Figs. 9 and 10. In Fig. 9, the square section data presented in Fig. 8 are combined with data for a roll angle of 45°, both sets of data being for a horizontal cavity. Bearing in mind that $\gamma = \pi/4$ corresponds to an extremum, it is clear that the effect of roll on heat transfer is very small. In the interest of clarity, intermediate data obtained for other roll angles have not been plotted.

Figure 10 shows the effect of tilt on heat transfer for the roll which displayed the lowest rates, i.e. $\gamma = \pi/4$. As indicated, a family of curves is generated with tilt angles above and below zero. The highest tilt angles reveal a gradual transition to a boundary layer type of flow even when $Ra = 10^5$, whereas the lower angles barely exhibit entry into the impeded regime. It is evident that large negative tilt angles are associated with effective insulation characteristics, at least for $Ra \lesssim 10^5$.

The open symbols in Fig. 8 suggest that the triangular section creates a less effective heat transfer system than the square section when the comparison is based on a Rayleigh number using the short side dimension D. Also shown in Fig. 8 (solid symbols) are the same triangular data based upon the hydraulic mean diameter $D/(\sqrt{2}/2+1)$. The two sets of data may thus be brought into closer alignment. However, such a re-definition does not completely eliminate effects caused by an altered flow area or flow pattern which, as noted earlier, may be substantial. Consequently, the dimension D has been used consistently in all the heat transfer comparisons discussed below.

Figure 11 shows corresponding heat transfer data for a horizontal, triangular section at various roll angles. As might be expected, the geometrical effect is greater than that evident in Fig. 9 for the square section. The orientation of the longest side, the diagonal, is evidently important; maximum heat transfer occurs when the diagonal is vertical while a horizontal diagonal corresponds to a minimum. This reflects the importance of secondary motion on heat transfer rate. The horizontal diagonal is particularly conducive to insulating behaviour.

The effect of tilt on heat transfer rate in a triangular section is shown in Fig. 12 with the roll angle being that which produced minimum heat transfer behaviour in the horizontal position. Once again, variations in the tilt angle produced a family of curves in which

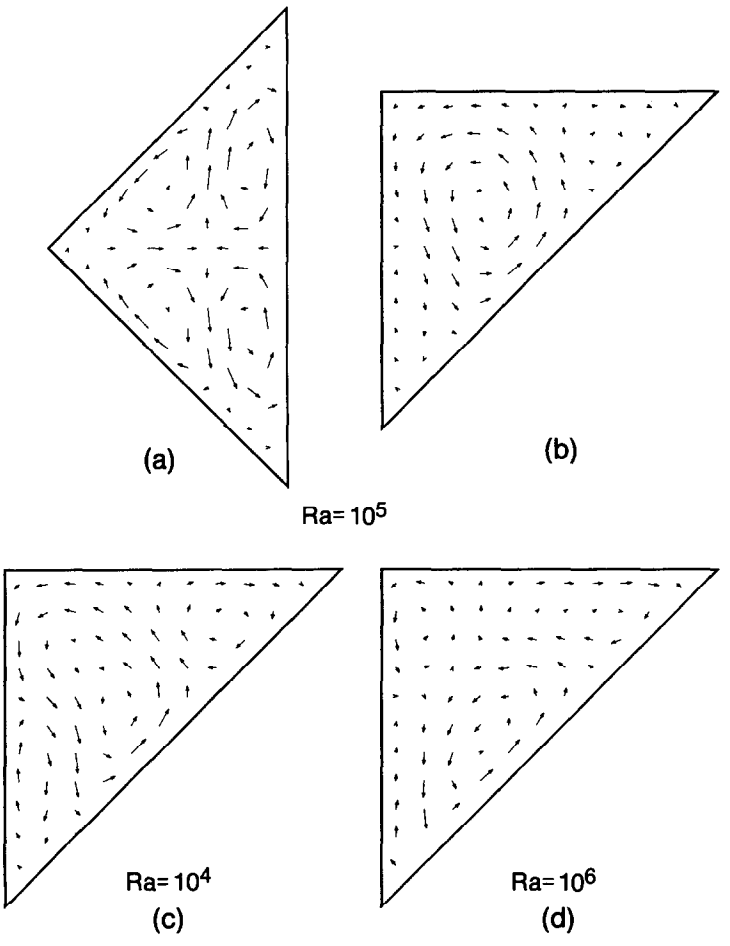

FIG. 7. Effect of roll on secondary flow in the central plan of a horizontal, triangular section cavity: $Ra = 10^5$.

only the lowest remain close to the conduction regime. As with the square section, the triangular section tilted at large negative angles is an effective insulator for $Ra < 10^5$.

Finally, the effect of the long wall boundary condition was explored by replacing $r_k = \infty$ with $r_k = 0$, i.e. using an adiabatic condition. The results generated have a lower accuracy (e.g. 10%) but serve well to illustrate the general trend. In Fig. 13, for example, the heat transfer data for the two extreme values of r_k indicate that the thermal conductivity of the wall will play an important role in a square section cavity which is aligned horizontally or with a positive tilt. Equally clear is the reduction of this effect when the tilt is made increasingly negative. In Fig. 14, which shows corresponding data for the triangular section cavity,

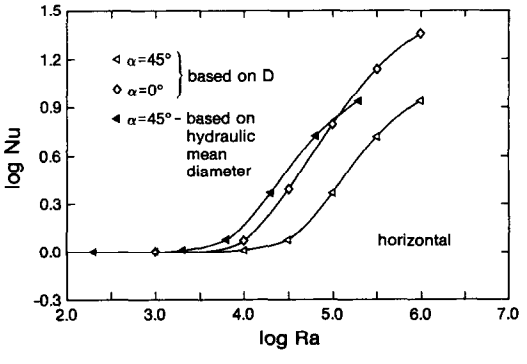

FIG. 8. Effect of Rayleigh number on heat transfer.

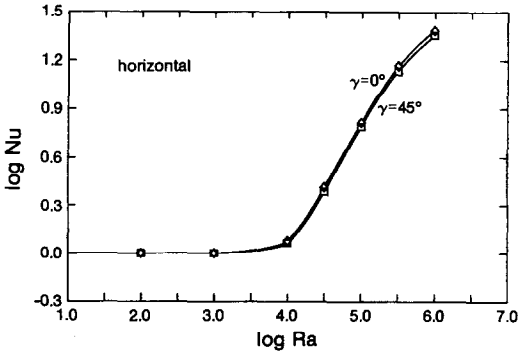

FIG. 9. Effect of roll on heat transfer: square section.

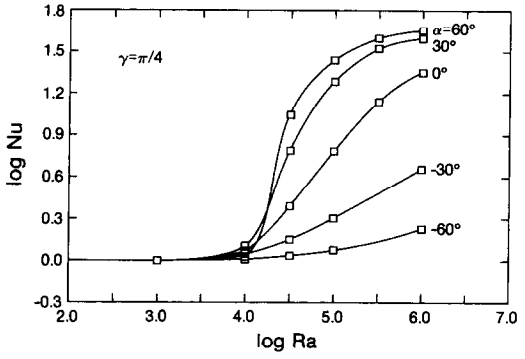

FIG. 10. Effect of tilt on heat transfer: square section.

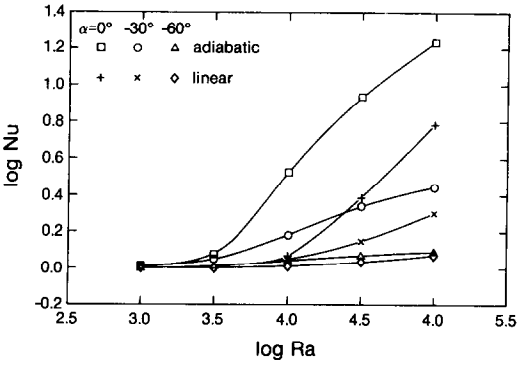

FIG. 13. Effect of wall conductivity on heat transfer in a square section cavity.

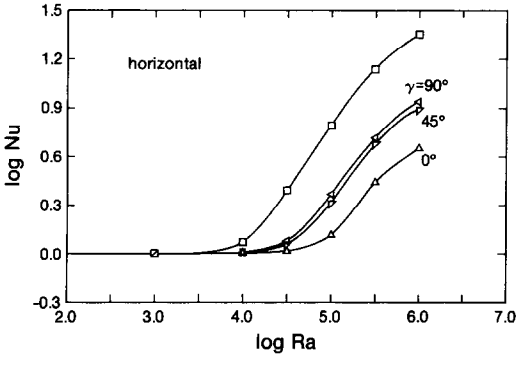

FIG. 11. Effect of roll on heat transfer: triangular section.

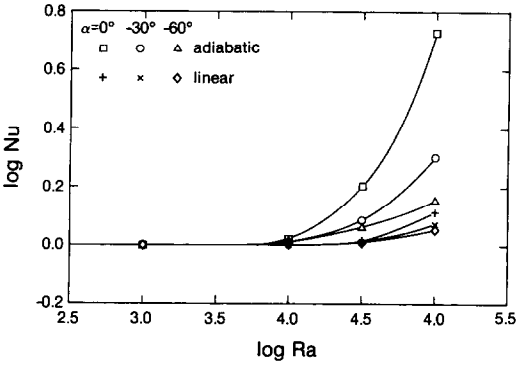

FIG. 14. Effect of wall conductivity on heat transfer in a triangular section cavity.

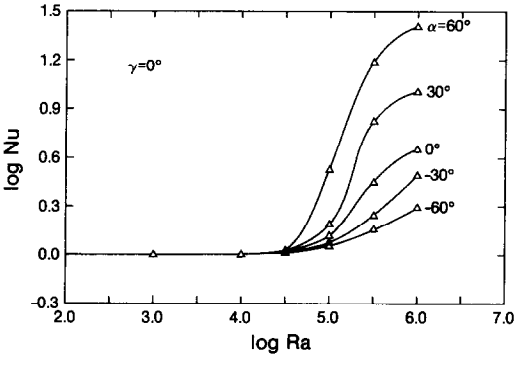

FIG. 12. Effect of tilt on heat transfer: triangular section.

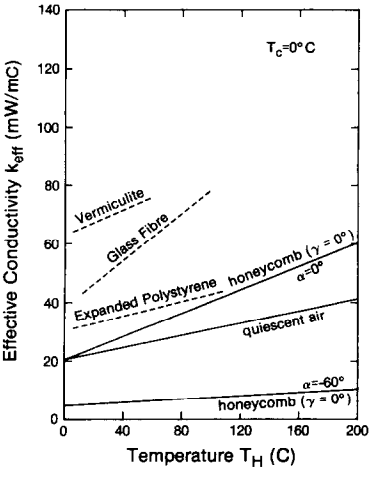

FIG. 15. Comparison of conductivities.

the effect is even more pronounced. For both cavity geometries, the precise boundary condition is seen to be unimportant under the desirable design condition of large negative tilt.

Comparison with conventional insulation

Figure 15 offers a comparison of the insulation characteristics of typical insulators [19] with the most effective system found in the present investigation. The effective conductivities k_{eff} in this figure are based on the area which an inclined honeycomb cavity projects on the containing walls. This definition introduces the paradox of conductivities lower than that of pure air, a feature resulting from tilted honeycombing. Such a feature in fact applies to any conductor inclined relative to the containing wall normal because the path length is then increased and the effective cavity cross section is reduced, but this reduction only applies if no heat flows laterally between the cavities. This tilting attenuation is not possible in insulation fillings which are essentially isotropic.

As indicated, the negatively-tilted cavity has a theoretical performance which is much better than that of representative conventional fillings. In practice, however, the honeycomb matrix would likely yield a higher conductivity because of lateral conduction; its performance would probably be closer to that of quiescent air.

CONCLUSIONS

The paper presents the results of a numerical study of flow and heat transfer in honeycomb wall spaces, the principal objective being an assessment of thermal insulating effectiveness. Using the discretized forms of the differential equations governing motion, continuity and energy, a finite-difference algorithm was employed in the development of numerical solutions for a slender cavity filled with air under steady, laminar conditions. No attempt was made to include the effects of radiation or leakage.

Exploration of the effect of the Rayleigh number on heat transfer indicated three regimes. For high Rayleigh numbers, i.e. $Ra > 10^6$, the $Nu \sim Ra$ relation suggested a boundary layer regime which gradually merged with an impeded regime as the Rayleigh number was reduced and the boundary layer filled the cavity. At much lower Rayleigh numbers, i.e. $Ra \leqslant 10^4$, the impeded regime degenerated into a conduction regime in which the velocity field had a negligible effect on the temperature field.

Two particular section geometries were studied—the square and the triangle. With the cavity horizontal, the effect of roll about the horizontal axis was found to be negligible for the square section and moderate for the triangular section. For the latter, the minimum heat transfer curve corresponded to the hypotenuse (diagonal) being horizontal, while for the former the minimum occurred with the diagonal at 45°.

Tilt of the cavity longitudinal axis relative to the horizontal produced much greater changes in heat transfer rate for tilt angles in the range $-60° < \alpha < 60°$. As anticipated, heat transfer rates increased with increasing tilt angle. Conversely, heat transfer rates decreased substantially with increasingly negative tilt angles. As $\gamma \to \pi/4$, the system approaches a one-dimensional, purely conductive state when the linear ($r_k = \infty$) and adiabatic ($r_k = 0$) boundary conditions coincide. This tendency was observed.

A comparison between conventional insulating fillings and the best insulating performance observed in this study suggests that honeycombing is a very effective thermal strategy. Production problems and the associated economics of manufacturing are beyond this paper, but should they not introduce any barriers the honeycomb wall may provide useful solutions to a variety of thermal and structural problems.

Acknowledgement—This work was supported by the Natural Sciences and Engineering Research Council of Canada to whom we are grateful.

REFERENCES

1. I. Catton, Natural convection in enclosures, *Proc. 6th Int. Heat Transfer Conf.*, Toronto, Vol. 6, pp. 13–43 (1978).
2. R. L. D. Cane, K. G. T. Hollands, G. D. Raithby and T. E. Unny, Free convection heat transfer across inclined honeycomb panels, *J. Heat Transfer* **99**, 86–91 (1977).
3. J. N. Arnold, D. K. Edwards and I. Catton, Effect of tilt and horizontal aspect ratio on natural convection in rectangular honeycombs, *J. Heat Transfer* **99**, 120–122 (1977).
4. L. M. Trefethen and K. C. Chung, The oneway heat wall—analysis and experiments on a vertical stack of inclined cavities, *Proc. 6th Int. Heat Transfer Conf.*, Toronto, Vol. 4, pp. 119–124 (1978).
5. K. C. Chung and L. M. Trefethen, Natural convection in a vertical stack of inclined parallelogrammic cavities, *Int. J. Heat Mass Transfer* **25**, 277–284 (1982).
6. J. Eftekhar, G. Darkazalli and A. Haji-Sheik, Conduction of heat across rectangular cellular enclosures, *J. Heat Transfer* **103**, 591–595 (1981).
7. G. S. H. Lock and J.-C. Han, Flow and heat transfer in a long, horizontal, rectangular cavity with differentially-heated ends, *Proc. 3rd Int. Symp. on Transport Phenom. in Thermal Control*, Taipei, pp. 299–311 (1988).
8. G. S. H. Lock and J.-C. Han, Buoyant laminar flow of air in a long, square-section cavity aligned with the ambient temperature gradient, *J. Fluid Mech.* **207**, 489–504 (1989).
9. T. S. Lee, Computational and experimental studies of convective fluid motion and heat transfer in inclined non-rectangular enclosures, *Int. J. Heat Fluid Flow* **5**(1), 29–36 (1984).
10. J. P. Coulter and S. I. Guceri, Laminar and turbulent natural convection within irregularly shaped enclosures, *Numer. Heat Transfer* **12**, 211–227 (1987).
11. E. M. del Campo, M. Sen and E. Ramos, Analysis of laminar natural convection in a triangular enclosure, *Numer. Heat Transfer* **13**, 353–372 (1988).
12. S. V. Patankar, *Numerical Heat Transfer*. Hemisphere, New York (1980).
13. J. P. Van Doormaal and G. D. Raithby, Enhancements of the SIMPLE method for predicting incompressible fluid flows, *Numer. Heat Transfer* **7**, 147–163 (1984).
14. J. W. Elder, Laminar free convection in a vertical slot, *J. Fluid Mech.* **23**(1), 77 98 (1965).
15. S. J. M. Linthorst, W. M. M. Schinkel and C. J. Hoogendoorn, Flow structure with natural convection in inclined, air-filled enclosures, *J. Heat Transfer* **103**, 535–539 (1981).
16. G. D. Mallinson and G. de Vahl Davis, Three-dimensional natural convection in a box: a numerical study, *J. Fluid Mech.* **83**, 1–31 (1977).
17. P. Bontoux, C. Smutek, B. Roux and J. M. LaCroix, Three dimensional, buoyancy-driven flows in cylindrical cavities with differentially-heated ends, Part I. Horizontal cylinders, *J. Fluid Mech.* **169**, 211–227 (1986).
18. P. Bontoux, C. Smutek, A. Randriamampianina, B. Roux, G. P. Extremet, A. C. Hurford, F. Rosenberger and G. de Vahl Davis, Numerical solutions and experimental results for three-dimensional buoyancy driven flows in tilted cylinders, *Adv. Space Res.* **6**(5), 155–160 (1986).
19. A.S.H.R.A.E., *Handbook of Fundamentals*. American Society of Heating Refrigeration and Air-conditioning Engineers, Atlanta (1985).

CONVECTION NATURELLE DANS LES ESPACES DE PAROI A NIDS D'ABEILLE

Résumé—On présente les résultats d'une étude numérique de convection naturelle laminaire dans une paroi à nids d'abeille remplie d'air. On veut comparer cette paroi avec la paroi conventionnelle à cavité remplie de matériau poreux. En utilisant les formes discrétisées des équations aux dérivées partielles, on obtient des résultats sur le transfert de chaleur pour deux cavités différentes : sections droites carrée et triangulaire, ayant toutes deux un rapport de forme de 5 : 1. On présente le nombre de NUSSELT en fonction du nombre de REYNOLDS. Trois régimes d'écoulement sont évidents. L'effet de rotation de la cavité autour de son axe longitudinal est examiné, avec l'effet d'inclinaison de cet axe au dessus ou au dessous de l'horizontale. La cavité triangulaire inclinée, avec la température la plus élevée à l'extrémité supérieure présente des propriétés d'isolation comparable aux remplissages des parois conventionnelles.

NATÜRLICHE KONVEKTION IN EINER WAND MIT WABENSTRUKTUR

Zusammenfassung—Es werden die Ergebnisse einer numerischen Untersuchung der laminaren natürlichen Konvektion in einer Wand mit Wabenstruktur vorgestellt. Dabei wird versucht, eine herkömmliche Wand, bei der Hohlräume mit porösem Material aufgefüllt sind, mit einer Wand ohne Hohlraumfüllung zu vergleichen. Durch numerische Lösung der diskretisierten Differentialgleichungen wird der Wärmetransport für quadratische und dreieckige Wabenquerschnitte bestimmt. In beiden Fällen wird ein Seitenverhältnis von 5 : 1 angenommen. Die Ergebnisse werden als Nusselt-Zahl über der Rayleigh-Zahl dargestellt. Dabei werden drei Strömungsformen erkennbar. Es werden die Einflüsse der Drehung der Hohlräume um die Längsachse sowie der Neigung der Längsachse untersucht. Im Falle eines dreieckigen Hohlraums, bei dem sich die warme Seite oben befindet, ergeben sich vergleichbare Wärmedämmeigenschaften wie bei einer herkömmlich gefüllten Wand.

ЕСТЕСТВЕННАЯ КОНВЕКЦИЯ В ПУСТОТАХ СТЕНКИ, ИЗГОТОВЛЕННОЙ ИЗ СОТОВОГО МАТЕРИАЛА

Аннотация—Представлены результаты численного исследования ламинарной естественной конвекции в хонейкомбовой стенке с заполненными воздухом сотами. Предпринята попытка сравнения хонейкомбовой стенки с обычной полостью, заполненной пористым веществом. С использованием дискретных форм определяющих дифференциальных уравнений получены данные по теплопереносу для двух различных поллостей, а именно, с квадратным и треугольным поперечными сечениями, отношения сторон которых равны 5 : 1. Данные представлены в виде графиков зависимости числа Нуссельта от числа Рэлея. Отмечены три режима течения. Исследованы эффекты вращения полости относительно ее продольной оси, а также наклона указанной оси вверх и вниз от горизонтали. Найдено, что изоляционные свойства наклонной треугольной полости с более высокой температурой у верхнего конца сопоставимы со случаем стенок с обычными наполнителями.